Rapid sealing of an alumina nanoporous network grown by anodizing and dye-filled

Vincent Cartigny, Delphine Veys-Renaux, Patricia Desenne, Emmanuel Rocca

Version of Record: https://www.sciencedirect.com/science/article/pii/S0257897219302464
Manuscript_34130dfa2fba7d5715079af75c29b6ff

Rapid sealing of an alumina nanoporous network grown by anodizing and dye-filled

Vincent CARTIGNY [1,2], Delphine VEYS-RENAUX [2], Patricia DESENNE [1], Emmanuel ROCCA [2]

[1] *Aptar Annecy (Graphocolor), 19, Av. des Vieux Moulins, 74000 Annecy*

[2] *Institut Jean Lamour, Université de Lorraine, UMR CNRS 7198, BP 70239, 54506, Vandeouvre-Lès-Nancy, delphine.veys-renaux@univ-lorraine.fr*

Abstract

In the field of indoor decorative items, aluminium alloys are widely used since their surface may be coloured by adsorption of dyes within an anodic nanoporous network. This anodizing/colouring process is followed by a sealing step ensuring the protection of the treated surface without modifying its aesthetic appearance.

In the present paper, water, nickel acetate and sodium silicate were used as sealing agents and implemented in rapid sealing processes dedicated to anodized then coloured aluminium surfaces. The morphological aspects were finely observed by scanning electron microscopy (SEM) and transmission electron microscopy (TEM). The elemental repartition was tracked by wavelength and dispersive spectrometry (WDS/EDS). The sealing efficiency was evaluated by electrochemical impedance spectroscopy (EIS) and a dye spot test. An optical characterization was performed by visible reflection spectrometry and gloss measurements.

Both water and nickel salt lead to the precipitation of a few tens of nanometers hydroxide layer, providing an efficient sealing in a short time while maintaining optical properties. Best performances are obtained with nickel salt. In contrast, the high adsorption of silicates inhibits the formation of the sealing superficial sheets on the one hand and even makes the dye desorb from the nanoporous oxide layer.

Keywords: anodic layer, sealing, SEM, EIS.

Introduction

Aluminium anodizing has been widely used as an industrial process to protect aluminium alloys from corrosion, but also to provide many decorative aspects for everyday objects in aluminium. Anodizing in acidic media produces on the surface of alloys a nanoporous oxide layer of several microns thickness [1–4], in which coloured pigments can be trapped, and with a variable roughness depending on surface preparation. The colouring is achieved by a chemical adsorption mechanism on the surface of nanometre pores during the immersion of the anodic film in a solution containing an organic or inorganic dye [5, 6]. A large range of tints may be reached and modulated by the thickness of the oxide layer. After colouring, desorption of the dye is prevented by performing a so-called sealing step that blocks the nanopores of the anodic oxide. The decorative applications of this surface treatment are numerous, particularly in the architecture field, for sporting instruments, for cosmetics packaging but also in aerospace [7].

Several sealing processes can be used to trap and block the dyes in the porous network. The simplest one is the hydrothermal sealing. It consists of immersing the anodized surface in deionized boiling water (T> 95 °C) for an estimated time of 2 min μm^{-1} [8], which generally leads to a long-time process. In boiling conditions, the reaction forms on the surface of the anodic oxide a coating of hydroxide sheets which is attributed to poorly-crystallized boehmite or aluminium hydroxide [9]. The most recent studies show that the hydratation of oxide and the hydrolysis of the aluminium sulphate induce a change in the chemical environment of aluminium cations from AlO_4 tetrahedra to AlO_6 octahedra, and the precipitation of the hydroxide sheets on the extreme surface [10]. Chromate-based sealing processes have been applied for their efficient anticorrosion properties but they are now excluded due to the high toxicity of Cr(+VI) salt [11]. In the last decades, nickel acetate-based sealing processes have been widely used for anticorrosion properties [12]. Especially for decorative applications, the sealing process using nickel salt in boiling conditions offers the advantages of a fast kinetic

[13] and an inconspicuous change of gloss and tint of the coloured pieces. Other sealing processes use fluoride anions which can substitute hydroxyl groups of the aluminium oxide by fluorine. This exchange leads to a local increase of the pH as shown by Chahboun et al [14, 15] on sealing with fluorozirconate salt. In the case of nickel sealing, the addition of fluoride allows the precipitation of nickel hydroxide on the top of the anodic oxide at low temperature (around 40°C) [12, 16, 17].

However, the use of heavy metal salts as nickel or fluoride anions should be now avoided due to health and safety regulations, and the management of the waste water reject in plants. In fact, nickel salts are now classified as possible CMR compounds and are responsible for some skin allergies [18].

In this context, the addition of several other metallic salts in boiling water (Co [19], Ce [20], Li [16]) or chemical compounds (such as triethanolamine [21]) have been considered in literature as alternatives to nickel salts without full success. Actually, the colouring/sealing process of aluminium anodic oxide must be efficient to trap the dye in the nanopores, without modifying the optical aspect (gloss and tint) and has to be carried out in a short time (several minutes) in the case of the surface treatment of mass consumer goods.

In this framework, the present paper is devoted to study both the properties of nickel-based sealing process of coloured aluminium anodic oxide and some possible environmental friendly alternatives of sealing for indoor decorative applications as cosmetic packaging.

For this purpose, the nanoporous oxide layers were obtained by anodizing in a sulfuric acid of 5657 aluminium alloy. Then, colouring was carried out by adsorption of an orange chromium-azoic dye to induce a golden colour, and was finished by a rapid sealing of 4 min in hydrothermal conditions. Three sealing formulations were compared: deionised water, a nickel acetate based solution and a silicate solution. After metallographic analyses by scanning electron microscopy (SEM) and transmission electron microscopy (TEM) coupled with energy dispersive X-ray spectroscopy (EDS) and wavelength-dispersive X-ray

spectroscopy (WDS), the efficiency of dye trapping in nanopores was characterized by electrochemical impedance spectroscopy (EIS) and dye spot test. Finally, the optical effect of sealing was evaluated by UV-visible absorption spectroscopy and visible reflection spectroscopy.

1. Materials and methods

1.1. Materials and coatings

AA5657 alloy laminated plates (Al: 98 wt.%, Mg: 0.9 wt.%, Si : 0.6 wt.% Si, Fe : <0.5 wt.%) were provided by Constellium. Firstly, plates were chemically etched with a classical brightening process in a solution containing phosphoric, nitric and sulfuric acids for 3 min at 95 °C [22]. ~~Then,~~ Plates were then washed for 1 min in a concentrated nitric acid solution at 25 °C. The anodizing process was performed in a two-electrode cell, the aluminium alloy substrate being mounted vertically between two lead counter electrodes. The nanopourous anodic layers were grown in H_2SO_4 2 M at room temperature, by applying constant voltage for 15 min. After rinsing, plates were immersed for 150 s in a colouring solution, an orange Cr-based azoic dye at a concentration of 0.15 g L^{-1} at 55 °C (Orange G from CLARIANT). Finally, the sealing step was achieved by a short immersion (only 4 min) in solutions heated at 95°C. Three different sealing formulations were chosen and compared:

- deionized water at pH = 6.8, further referred as “water” sealing,
- a nickel acetate salt solution containing 2 g L^{-1} of nickel metal, further referred as “nickel” sealing : 2 min of immersion in the nickel acetate solution are followed by 2 min in boiling deionised water,
- a solution of sodium silicate (Na_2SiO_3 provided by Alfa Aesar) acidified until pH = 10 by addition of silicic acid ($Si(OH)_4$ provided by Sigma-Aldrich), further referred as “silicate” sealing (the total silicon concentration was 5.10^{-3} M).

1.2. Physicochemical characterization

The sealed anodic oxides were observed with a Hitachi S-4800 FEG-SEM at an acceleration voltage of 1 or 2 kV in order to be sensitive to the extreme surface morphology. Cross sections were prepared with an ion beam polisher (JEOL IB-09010CP) and then analysed in a JEOL J7600F FEG-SEM, coupled with both EDS and WDS spectroscopies. A finer cross-section analysis was carried out in a JEOL ARM 200F TEM (by using STEM mode and EDS for chemical mapping) after preparation of the sample thanks to a MEB with focused ion beam (FEI Helios Nanolab 600i).

1.3 Electrochemical characterization

Electrochemical characterization of the samples was performed in a non-corrosive K_2SO_4 0.5 M electrolyte, by using a classical three-electrode set-up, with the working electrode mounted at the bottom of the cell, facing to a platinum grid used as a counter electrode and a saturated calomel electrode used as a reference. The electrochemical set-up was driven by a Gamry REF600 potentiostat. After 2 hours of maintain at the open-circuit potential (to monitor the electrochemical interface steady state), electrochemical impedance spectroscopy measurements were recorded over the frequency range 1 MHz to 1 mHz with a voltage magnitude of 20 mV. Impedance spectra were fitted with ZsimpWin software [23] over the limited frequency range 100 kHz to 100 mHz, in order to get a relevant fit of the data with the chosen equivalent circuit.

1.4 Spot dye test

The performance of the sealing was evaluated by the ISO 2143 dye spot test [24]. The surface of the sealed and unsealed samples was degreased with ethanol and a spot of H_2SiF_6 0.09 M solution was deposited to dissolve the coating. After 1 min, the surface was rinsed with water and a spot of Sanodal red B3LW dye from CLARIANT at pH = 5.7 (10 $g.L^{-1}$) was deposited

on the previously attacked area. After 1 min, a new water rinse was performed to remove the excess of dye. The resulting color spot was observed and compared with a tint scale numbered from 0 to 5. The lowest index is assigned to a very effective sealing. On the contrary, an index of 5 corresponds to an unsealed layer.

1.5 Optical characterization

The acquisition of the UV-visible absorption spectrum of dye was made on a 0.15 g L^{-1} concentrated solution with a JASCO V-730 spectrophotometer. The optical properties of the surfaces were characterized by reflection spectrometry measurements in a Konica Minolta CM-5 spectrophotometer, by using a diaphragm with a diameter of 30 mm and excluding the specular reflection (SCE mode). Gloss measurements were performed as well by using a three-angle (20°/40°/85°) Rhopoint IQ goniophotometer at 540.1 nm. The glossmeter measures the light intensity of the specular reflection of the sample with respect to a reference surface, a black glass. The result is expressed in gloss unit (GU), according to the relation: $\mathbf{Gloss} = \mathbf{100}\ \frac{\mathbf{Reflection\ (sample)}}{\mathbf{Reflection\ (standard)}}$. The reflection measurement is carried out at different angles regarding the normal of the interface.

2. Results

2.1. Morphology of unsealed and sealed dye-filled anodic layers

Fig.1 illustrates the extreme surface morphology of unsealed (Fig.1a) and sealed (Fig.1b to d) dye-filled anodic layers. According to Fig.1a, the colouring step only induces an internal filling of the alumina nanoporous network, without external physical blockage of the pores which remain open. Actually, the observed morphology is very similar to the extreme surface of a not coloured anodized layer, with columnar porosities of about 10 nm diameter [1, 25]. On the surface observation of anodized and coloured samples immersed for only 4 minutes in “water” (Fig.1b) or “nickel” (Fig.1c) solutions, the nanostructured network disappears since

the columnar nanostructure is covered by a sealing film. This overlayer is made of sheets whose morphology looks like hydroxide sheets formed by the conversion of nanoporous alumina into boehmite [26]. In the specific case of nickel sealing, the covering is more homogeneous and the sheets are finer than in the film formed in water. Contrary to the external physical blockage of the columnar alumina reached with water or nickel sealing, no formation of superficial film can be observed after 4 minutes of immersion in the silicate containing formulation (Fig.1d). The observed morphology lets appear the typical nanoporous network of anodic and dye-filled anodic layers.

A fine observation of sealed layers cross-sections was performed by TEM as depicted in Fig. 2. From the morphological point of view, the dye-filled anodized oxide coating consists of a ten nanometres' thick internal barrier layer surmounted by a columnar porous structure of several microns, perpendicular to the aluminium surface (Fig. 2a). The global morphology is very similar to what is usually observed on anodized aluminium and seems to be unaffected by dye-filling and sealing in depth [1]. Regarding the extreme surface, a modification of the ten upper nanometres is nevertheless obvious in cases of water sealing (Fig.2b) and nickel sealing (Fig.2c). Consistently with the SEM surface micrographs (Fig.1b and 1c), the extreme surface consists of nanometre tangled sheets, likely hydroxide sheets. According to local electron diffraction in MET, these covering products are amorphous. On the opposite, after immersion in the silicate containing formulation, the top of the anodized and dye-filled layer show the porous nanostructure without formation of any overlayer (Fig.2d).

3.2. Chemical analysis of the sealed oxide layers

As revealed by chemical analyses (Fig.3 and Fig.4) and also referred elsewhere [10] the anodized layer is mainly made of aluminium and oxygen (Fig.3), but also contains sulphur, with an homogeneous content of about 3 at.% in all the depth, corresponding to the incorporation of sulphates from the electrolyte (Fig.4).

In the cases of sealing with formulations containing nickel salt or silicate salt, both elements nickel and silicon are integrated within the anodic film (Fig. 4a and Fig. 4b).

In nickel sealed layer, nickel is mainly located in the upper part of the coating until 8 at.% (revealed by EDS analysis in TEM), forming a superficial overlayer with a thickness of around 20 nm (Fig. 3). In depth, nickel is also present within the columnar nanoporous structure until 2 µm (Fig. 4a) with a content below 1 at.%, as revealed by EDS analysis in SEM. Nevertheless, inside the nanoporous network, the nickel content can reach 15 to 20 at.% in some places (Fig 3). Sulphur seems to be more concentrated in the 20 upper nanometres (about 4 at.% according to EDS measurements performed in TEM). Underneath this top most layer, depletion in sulphur (2 at.%) is observed over about 2 microns depth (Fig. 4a) and the sulphur concentration regains then its usual value in anodic films grown in sulphuric acid (3 at.%).

Sealing with silicates induces the penetration of silicon within the porous layer as well (Fig. 4b), not limited to the two first microns but until the oxide metal interface. Contrary to what is measured for nickel sealing, the sulphur content remains constant in the oxide depth (around 3 at.%) and no specific desorption can be observed from the outer part.

3.3. Electrochemical behaviour of the unsealed and sealed dye-filled anodic layers in non-corrosive medium

Electrochemical impedance spectroscopy was carried out in a non-corrosive medium in order to evaluate the efficiency of the different sealing processes and to provide details on the sealing mechanisms. Bode representations are drawn in Fig. 5.

Spectra can be first qualitatively interpreted by comparing the value of modulus in different frequency ranges (Fig. 5a). The modulus value at high frequency is known to be characteristic for the global resistance of electrochemical interface, which seems to be not significantly modified by any kind of considered sealing process. Actually, the efficiency of the sealing is

characterized by an increasing of the modulus value in the middle frequency range, associated with a phase shift [29]. This modulus increase corresponds to an increase of resistance to ionic diffusion through the porous layer by the presence of the "sealed" layer.

As referred in the literature [26–28], the spectra recorded on sealed anodic film can be modelled by using an equivalent electrical circuit composed of two time constants (Fig. 6), represented by two *RC* loops in series with the electrolyte resistance R_e. The one at low frequency can be assigned to the dielectric relaxation of the internal barrier layer (R_b, C_b) and the other at high frequency corresponds to the porous layer (R_p, C_p). The electrical parameters deduced from the fit of the experimental spectra are gathered in Table 1.

The value of the barrier layer resistance R_b is very high, around 10^9 **Ω** cm^2 [30] and is not significantly modified by the sealing processes. By considering this barrier layer as a planar dielectric, its capacitance C_b may be related to its thickness by the relation, $C_b = \frac{\varepsilon\, \varepsilon_0\, S}{d_b}$, where d_b is the thickness of the barrier layer, ε is the dielectric constant of the medium (ε_{Al2O3} = 10), ε_0 is the dielectric constant of vacuum, S is the active area. The calculation leads to an estimation of the barrier layer of around 12 nm (with C_b = 8.3 10^{-7} $F.cm^{-2}$), in agreement with TEM observations (fig. 2a).

Consistently with the first qualitative observations, the resistance assigned to the ionic diffusion through the porous layer R_p, is enhanced by water and nickel sealing processes, reaching 2 to 4 10^4 **Ω** cm^2, namely one order of magnitude higher than without sealing. The R_p increase by a ten factor is sufficient to trap and block the dye molecule inside the nanoporous network as shown by the index of dye-spot test of about 2-3. This result is well-corroborated by the observation of a nanometre more or less compact layer on the top of nanopores. By contrast, R_p is only slightly increased by silicate sealing, almost similar to the one without sealing. In comparison, the dye-spot test shows a 5 index value, corresponding to a not-sealed anodic oxide, correlated with the absence of compact top layer in the case of silicate sealing.

The pore capacitance values, C_p, undergo a drastic increase after water and nickel sealing, which can be assigned to a decrease of permittivity and ionic conductivity inside the nanpores. As observed for the R_p value, the C_p value is only slightly modified by the silicate sealing, which confirms that the silicate sealing has a poor effect on the electrochemical behaviour the aluminium anodic oxide.

3.4. Optical properties of the unsealed and sealed nanoporous oxide layers

The optical properties of anodized/coloured/sealed surfaces depend on two key factors. The tint is first given by the absorption of the dye in the UV-visible spectra (Fig. 7 and Fig. 8), and the reflections of the light on metal oxides and on underlying metallic substrate lead to a specific brightness or gloss of the surface [31] (Fig. 9). Both tint and brightness may be modified by the sealing processes, leading to a change of the colour of the samples.

According to Fig. 7, the orange G dye exhibits an absorption band in the UV-visible range with a maximum at 470 nm. This wavelength corresponds exactly to the minimum of reflection observed on the unsealed sample and the samples sealed with water and nickel, demonstrating the presence of the orange dye G inside the nanopores. While the spectrum recorded on the sample sealed with water is identical to the one on the unsealed sample at any point, small deviations can be observed due to the presence of nickel in the sealing film. In the specific case of sealing with silicates, the orange G dye has obviously desorbed from the nanoporous network since the reflection minimum corresponding to the presence of the dye has disappeared.

The brightness of the different surfaces was evaluated by gloss measurements and the results obtained for three different angles are given in the Fig. 9. The anodized samples are usually very bright, essentially due to the chemical polishing. Consequently, no significant difference in the gloss level can be evaluated with high grazing angle (85°) and only measurements performed at 20° and 60° provide relevant results. For both incident angles, the same trend

can be described. In comparison with the unsealed sample, nickel and silicate sealing processes induce more scattering and a consequent loss of gloss, because of the presence of the more or less rough layer composed of nanometre hydroxide sheets. This effect remains nonetheless very slight. On the opposite, the sealing process with silicates seems to lead to higher level of gloss regarding the unsealed sample. This observation is explained by the loss of the incorporated dye, which increases the reflected intensity and artificially increases the gloss level.

3. Discussion and mechanisms

Most of the studies on hydrothermal sealing are based on long time sealing, usually several tens of minutes, which suggest that the formation of a sealing film is a long-time process [27, 32]. According to the results presented in this paper, a short sealing time of 4 min is sufficient to induce the formation of a top-layer over the nanoporous anodic network in the cases of water and nickel sealing. The formation of the hydrothermal sealing films involves the dissolution of aluminium ions from the anodic film and a pH decrease, because of hydrolysis of the aluminium sulphate compounds, according to the following reaction:

$Al_2(SO_4)_3 + 2\ H_2O \rightarrow 2\ Al(OH)^{2+} + 2\ H^+ + 3\ SO_4^{2-}$

However, after the short sealing, EDS analysis shows that the anodic film still contains nearly 3 at.% of sulphur, due to the presence of sulphates (Fig.4). Moreover, reflection spectra are not modified by hydrothermal sealing (Fig.8), indicating that the hydrolysis of sulphates does not provoke any desorption of the dye during immersion in boiling water. In a second step during sealing, aluminium hydroxide precipitates at the top of the layer in the form of hydroxide sheets to form the sealing or blocking layer, as suggested by Rocca et al [10]:

$Al(OH)^{2+} + 2\ H_2O \rightarrow Al(OH)_3 + 2\ H^+$

In 4 minutes, without nickel ions, the sealing layer is formed by aluminium hydroxide sheets of about 100 to 200 nm which partially cover the nanoporous oxide network. On the surface,

this nanometre layer induces a slight loss of gloss recorded at 20° and 60° (Figure 9) by light scattering. Even though this rapid sealing does not completely seal the nanopores according to morphological observations, it provides a significant increase of the pore resistance as revealed by electrochemical impedance spectroscopy. The reached R_p value is sufficient to block the dye molecules inside the pores as confirmed by the qualitative dye-spot test.

In the case of hydrothermal sealing with Ni^{2+} acetate addition at pH=5, the hydroxide sheets on the surface are thinner than without nickel, about 50 nm (Fig. 1c). The elementary mapping and the concentration profile of the nickel-sealed oxide show that the nickel sealing does not result from a precipitation of $Ni(OH)_2$, as it is often mentioned in the literature for long-time sealing processes [33]. Indeed, nanoscale elementary mapping (Fig. 3) shows that nanopores are covered and partially filled with compounds containing nickel, oxygen and sulphur.

The lower sulphur content on the first micrometres of the oxide reveals that the hydrolysis of the sulphates occurs during the sealing process, which explains the formation of sulphur-containing precipitates. In pores, some nickel precipitates can contain until 15 to 20 at.% of nickel by EDS analysis in TEM inside the nanometre pores. This kind of composition could correspond to the precipitation of nickel hydroxysulfate compounds, as already studied in literature in hydrothermal conditions [34], which can be formed according the following reaction:

$$Ni^{2+} + (2-x)\ OH^- + x\ SO_4^{2-} \leftrightarrow Ni(OH)_{2-x}(SO_4)_x.$$

Moreover, impedance spectroscopy shows that the pore resistance reaches a 43 kΩ.cm² value, which is sufficient to trap the dye molecules inside the pores according to the dye spot test. Simultaneously, the growth of hydroxide sheets is probably inhibited by the rapid covering of the nanoporous oxide network by nickel precipitates. Consequently, the gloss loss remains very low, and the optical properties of surface are quasi-unchanged compared to an unsealed sample.

Regarding the hydrothermal sealing in presence of silicates at pH=10, the concentration profile of silicon shows that the diffusion and adsorption of silicates occur throughout the entire depth of the nanoporous network (Fig. 4b). In addition, the reflection spectrum of the sealed surface clearly shows that the dye molecules have also quasi-entirely desorbed from the nanoporous structure (Fig. 8).

The question is: "how silicates can be adsorbed on aluminium anodic oxide at pH=10?" Actually, given that the isoelectric point (PZC) of anodic aluminium oxide is around pH=8.5-9, the surface of the aluminium oxide should be predominantly covered by Al-O^- sites at pH=10 [25, 4], which is theoretically unfavourable for the formation of a silicates adsorption film. It is well-known for example that the adsorption of anions such as phosphate is very difficult even impossible on alumina at pH over 8 [36]

However, Gaggiano and al [37] have suggested that the presence of sodium cations can hide the charge of anionic sites on oxide and allow the adsorption of silicate anions on the negative site of the aluminium oxide. Moreover, in the case of anodized aluminium oxide, the hydrolysis of aluminium sulphate naturally induces a decrease of pH inside the nanometre pores, which could favour the presence of Al-OH and Al-OH_2^+ cationic sites. This pH decrease inside the pores could explain the important adsorption of silicate throughout the porous network.

On the other hand, the presence of silicate in the nanoporous network prevents the formation of hydroxide sheets or blocking nanometre layer as observed for water sealing or nickel sealing, which suggests that the release of aluminium ions is prevented by the silicate adsorption, probably due to stability of the bond between silicate and aluminium cations. Consequently, the formation of the hydroxide sheet layer, resulting from the hydrothermal sealing reaction, is quasi-entirely inhibited by the silicate adsorption. This observation is well-corroborated by the electrochemical impedance measurements which show a very low increase of the R_p resistance in comparison with the unsealed sample.

4. Conclusions

For indoor decorative applications, an efficient sealing process of anodized/coloured aluminium requires a hydrothermal reaction of the aluminium oxide, but desorption of the dye molecules and morphological modification of the extreme surface must be avoided.

From the chemical point of view, the different ions release (aluminium, sulphate) induces the precipitation of sealing products which should not affect the optical properties of the surface.

- Nickel sealing is more effective than water sealing, even over a short time. Actually, hydroxide sheets of smaller size are obtained with the nickel salt. They cover more homogeneously the surface and partially fill the top of nanopores by the precipitation of nickel hydroxysulphates.
- The brightness of the anodized / coloured surface is slightly modified by the precipitation of the hydroxide sheets which induce light scattering, with an effect depending on their size.
- The immersion of the coloured aluminium oxide in a silicate solution leads to a rapid desorption of the dye. The nanoporous network is not sealed but a layer of chemisorbed silicates is present on walls of the nanoporous network, which inhibits the formation of hydroxide sheet sealed layer.

Acknowledgements

Special acknowledgements are due to Jaafar Ganbaja for MET observations, Lise Salsi and Andréi Lecomte for MEB observations and analysis.

References

[1] G.E. Thompson, Porous anodic alumina: fabrication, characterization and applications, Thin Solid Films. 297 (1997) 192–201.

[2] M.M. Lohrengel, Thin anodic oxide layers on aluminium and other valve metals: high field regime, Mater. Sci. Eng. R Rep. 11 (1993) 243–294.

[3] V.P. Parkhutik, V.I. Shershulsky, Theoretical modelling of porous oxide growth on aluminium, J. Phys. Appl. Phys. 25 (1992) 1258–1263.

[4] S.J. Garcia-Vergara, P. Skeldon, G.E. Thompson, H. Habazaki, A flow model of porous anodic film growth on aluminium, Electrochimica Acta 52 (2006) 681–687.

[5] M. Franco, S. Anoop, R. Uma Rani, A.K. Sharma, Porous Layer Characterization of Anodized and Black-Anodized Aluminium by Electrochemical Studies, ISRN Corros. 2012 (2012) 1–12.

[6] A. Hakimizad, K. Raeissi, F. Ashrafizadeh, A comparative study of corrosion performance of sealed anodized layers of conventionally colored and interference-colored aluminium, Surf. Coat. Technol. 206 (2012) 4628–4633.

[7] Y. Goueffon, C. Mabru, M. Labarrère, L. Arurault, C. Tonon, P. Guigue, Mechanical behavior of black anodic films on 7175 aluminium alloy for space applications, Surf. Coat. Technol. 204 (2009) 1013–1017.

[8] J.S. Safrany, Anodisation de l'aluminium et de ses alliages, Tech. Ing. Corros. Vieil. (2001) M1630–1.

[9] R.K. Hart, A study of boehmite formation on aluminium surfaces by electron diffraction, Trans. Faraday Soc. 50 (1954) 269.

[10] E. Rocca, D. Vantelon, A. Gehin, M. Augros, A. Viola, Chemical reactivity of self-organized alumina nanopores in aqueous medium, Acta Mater. 59 (2011) 962–970.

[11] M. Kendig, R.G. Buchheit, Corrosion inhibition of aluminum and aluminum alloys by soluble chromates, chromate coatings, and chromate-free coatings, Crit. Rev. Corros.

Sci. Eng. (2003) 379–399.

[12] B.R. Cheng, L. Hao, Comparative study of the effects of sealing processes on the wear resistance and the sealing quality of hard anodic coatings, Met. Finish. 98 (2000) 48–55.

[13] M. Kim, H. Yoo, J. Choi, Non-nickel-based sealing of anodic porous aluminum oxide in NaAlO2, Surf. Coat. Technol. 310 (2017) 106–112.

[14] M. Etienne, E. Rocca, N. Chahboun, D. Veys-Renaux, Local evolution of pH with time determined by shear force-based scanning electrochemical microscopy: surface reactivity of anodized aluminium, electroanalysis. 28 (2016) 2466–2471. doi:10.1002/elan.201600294.

[15] N. Chahboun, E. Rocca, D. Veys-Renaux, M. Augros, M. Boutoba, N. Caldeira, Sealing of anodized multiphase aluminum alloys with Cr(+III)/Zr(+IV) salts: characterization and corrosion behavior, J. Electrochem. Soc. 163 (2016) C69–C75.

[16] T. Koerner, method of compacting anodized metals with lithium lithium and fluoride contening solutions without using heavy metals, US5891269A, 1997.

[17] M.R. Kalantary, D.R. Gabe, D.H. Ross, A model for the mechanism of nickel fluoride cold sealing of anodized aluminium, J. Appl. Electrochem. 22 (1992) 268–276.

[18] C. Lid, Occupational contact dermatitis due to nickel allergy, (n.d.) 3.

[19] F. P Stiller, US2888388A, 1957.

[20] Y. Xingwen, C. Chunan, Y. Zhiming, Application of rare earth metal salts in sealing anodized aluminum alloy, J. Mater. Sci. Lett. 19 (2000) 1907–1908.

[21] A. Bautista, J.A. Gonzalez, Influence of triethanolamine additions on the sealing mechanism of anodised aluminium, Surf. Coat. Technol. (2001) 49–54.

[22] ASM international, aluminium and aluminium alloys, 1993.

[23] B. Boukamp, A Nonlinear Least Squares Fit procedure for analysis of immittance data of electrochemical systems, Solid State Ion. 20 (1986) 31–44.

[24] Dye spot test with prior acid treatment, NF EN ISO 2143, 2017.

[25] E. Rocca, D. Vantelon, S. Reguer, F. Mirambet, Structural evolution in nanoporous anodic aluminium oxide, Mater. Chem. Phys. 134 (2012) 905–911.

[26] V. López, M.J. Bartolomé, E. Escudero, E. Otero, J.A. González, Comparison by SEM, TEM, and EIS of hydrothermally sealed and cold sealed aluminum anodic oxides, J. Electrochem. Soc. 153 (2006) B75.

[27] G. Yoganandan, J.N. Balaraju, C.H.C. Low, G. Qi, Z. Chen, Electrochemical and long term corrosion behavior of Mn and Mo oxyanions sealed anodic oxide surface developed on aerospace aluminum alloy (AA2024), Surf. Coat. Technol. 288 (2016) 115–125.

[28] K. Bonnel, C. Le Pen, N. Pébère, E.I.S. characterization of protective coatings on aluminium alloys, Electrochimica Acta. 44 (1999) 4259–4267.

[29] M.J. Bartolomé, V. López, E. Escudero, G. Caruana, J.A. González, Changes in the specific surface area of porous aluminium oxide films during sealing, Surf. Coat. Technol. 200 (2006) 4530–4537.

[30] D. Veys-Renaux, N. Chahboun, E. Rocca, Anodizing of multiphase aluminium alloys in sulfuric acid: in-situ electrochemical behaviour and oxide properties, Electrochim Acta. 211 (2016) 1056–1065.

[31] S. Van Gils, P. Mast, E. Stijns, H. Terryn, Colour properties of barrier anodic oxide films on aluminium and titanium studied with total reflectance and spectroscopic ellipsometry, Surf. Coat. Technol. 185 (2004) 303–310.

[32] J.A. González, V. López, E. Otero, A. Bautista, Post sealing Changes in porous aluminum oxide films obtained in sulfuric acid solutions, J. Electrochem. Soc. 147 (2000) 984.

[33] L. Hao, B.R. Cheng, Sealing processes of anodic coatings—past, present, and future, Met. Finish. 98 (2000) 8–18.

[34] S. Vilminot, M. Richard-Plouet, G. André, Hydrothermal synthesis in the system $Ni(OH)_2$-$NiSO_4$: nuclear and magnetic structure and magnetic properties of

$Ni_3(OH)_2(SO_4)_2(H_2O)_2$, Inorg. Chem. 42 (2003) 6859-6867

[35] P.V. Brady, Alumina surface chemistry at 25, 40, and 60 °C, Geochim. Cosmochim. Acta. 58 (1994) 1213–1217.

[36] Y.-S.R. Chen, J.N. Butler, W. Stumm, Adsorption of phosphate on alumina and kaolinite from dilute aqueous solutions, J. Colloid Interface Sci. 43 (1973) 421–436.

[37] R. Gaggiano, P. Moriamé, M. Biesemans, I. De Graeve, H. Terryn, Mechanism of formation of silicate thin films on porous anodic alumina, Surf. Coat. Technol. 205 (2011) 5210–5217.

Table 1. Parameters obtained by the fitting of the EIS data of sealed and unsealed oxide layers in 0.5 M K_2SO_4 with the equivalent circuit described in Fig. 6.

Sealed layer	χ^2	C_b / F.cm^{-2}	R_b / Ω.cm²	C_p / F.cm^{-2}	R_p / Ω.cm²	Dye spot index
Without sealing	1.10^{-3}	$8.3\ 10^{-7}$	$9.7\ 10^{8}$	$2.7\ 10^{-6}$	$2.4\ 10^{3}$	5
Water	8.10^{-4}	$8.2\ 10^{-7}$	$9.4\ 10^{8}$	$1.5\ 10^{-8}$	$2.5\ 10^{4}$	3
Nickel	5.10^{-4}	$7.6\ 10^{-7}$	$7.5\ 10^{8}$	$6.5\ 10^{-9}$	$4.3\ 10^{4}$	2
Silicate	5.10^{-3}	$8.1\ 10^{-7}$	$3.0\ 10^{8}$	$4.1\ 10^{-7}$	$4.9\ 10^{3}$	5

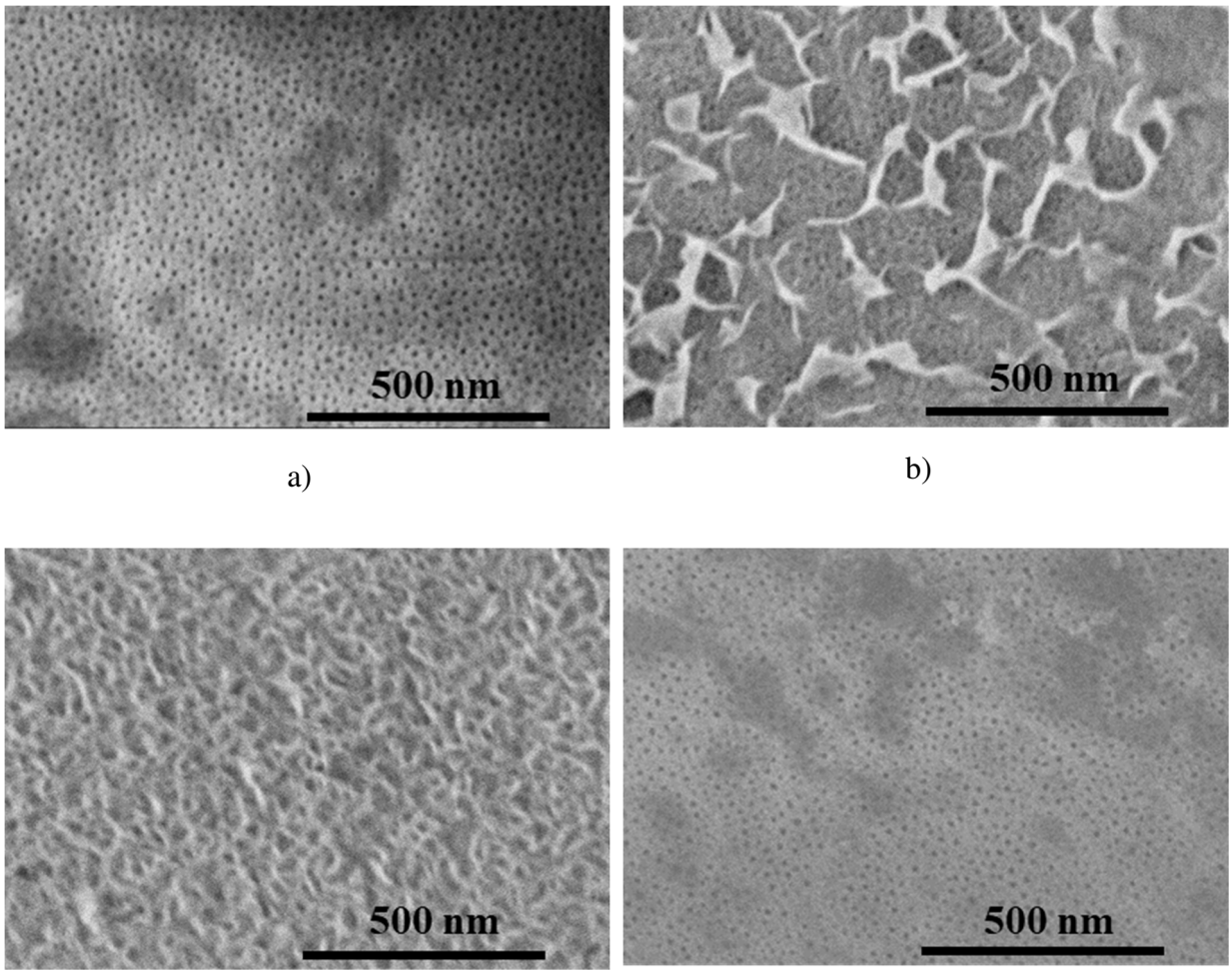

Fig. 1. FEG-SEM surface views of anodized / coloured samples without sealing (a), with water sealing (b), with nickel sealing (c) and with silicate sealing (d).

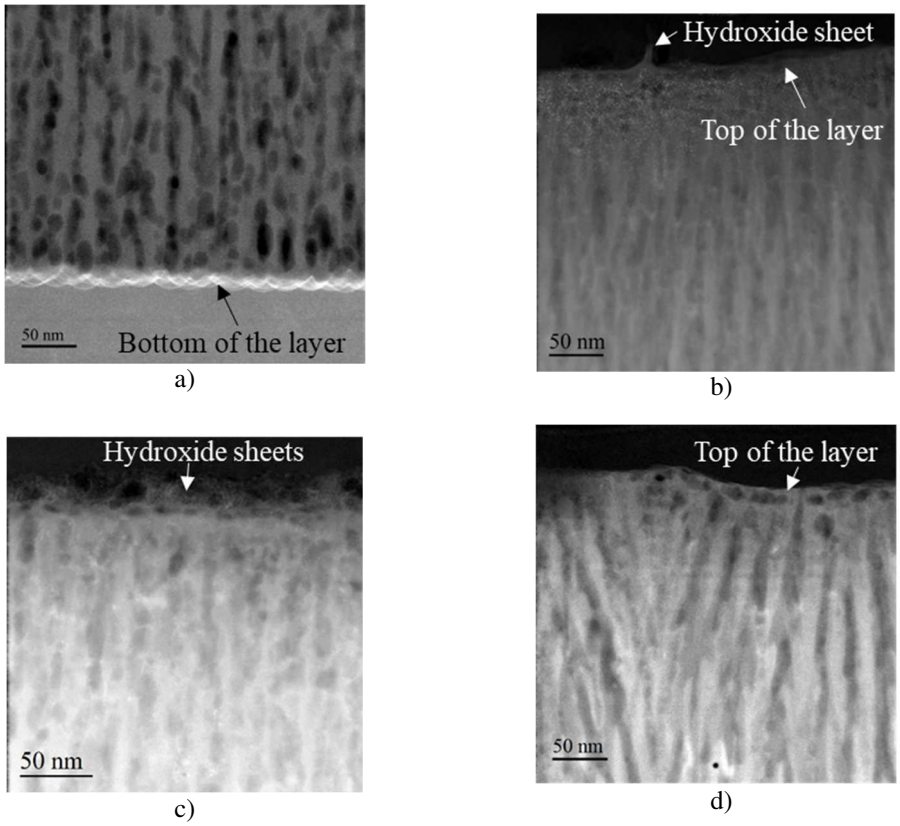

Fig. 2. Cross sections dark field TEM observations of anodized / coloured layers after 4 minutes of sealing: typical bottom of the layer (a), top of the layer after water sealing (b), nickel sealing (c), silicate sealing (d).

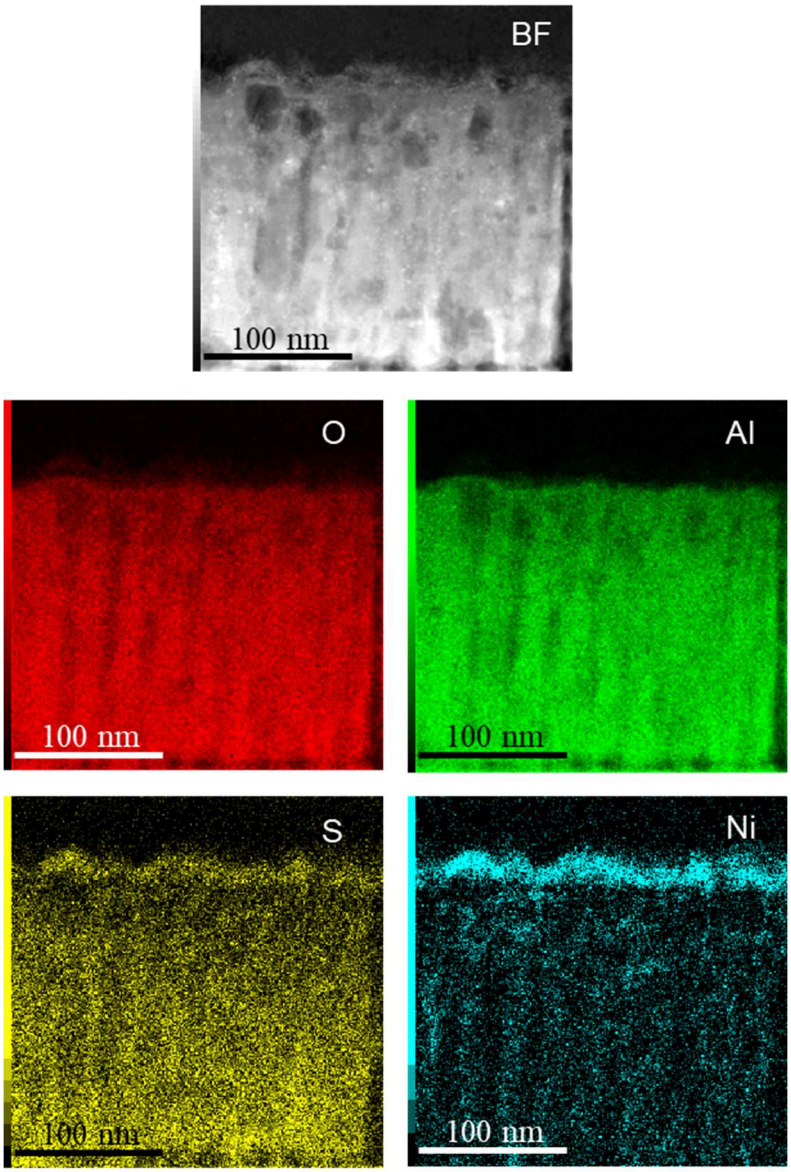

Fig. 3. Characterization in a TEM of the upper part of an anodized / coloured layer sealed for 4 minutes in a nickel acetate solution: bright field micrograph and EDS mappings of O, Al, S and Ni.

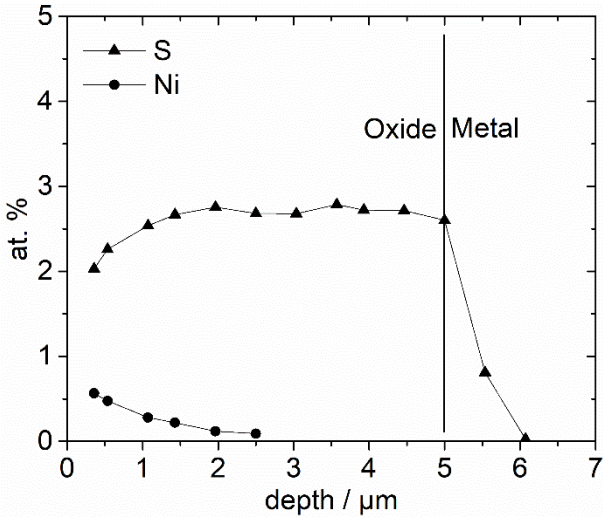

a)

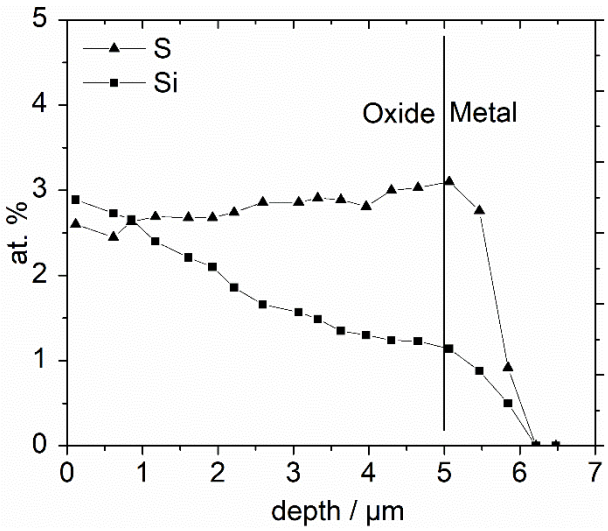

b)

Fig. 4. Concentration profiles measured by EDS in the anodic layer sealed by nickel (a), silicate (b).

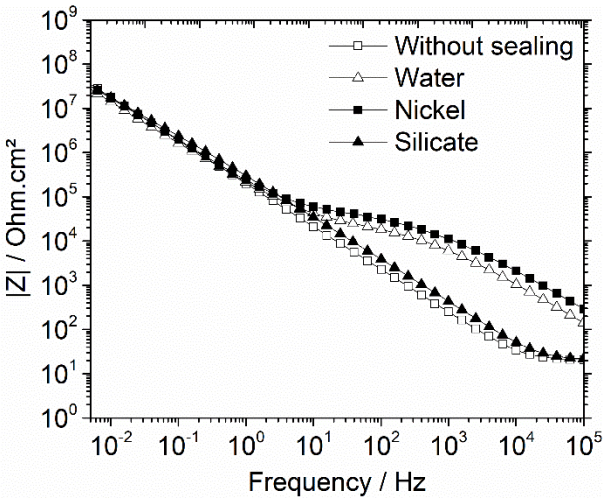

a)

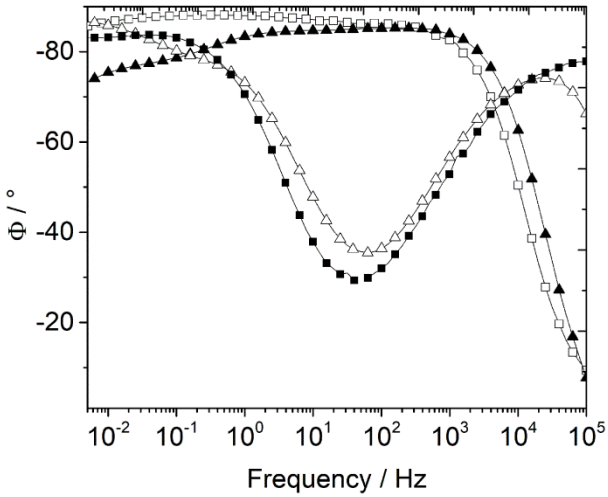

b)

Fig. 5. Bode representations of EIS data recorded in K_2SO_4 0.5 M on unsealed and sealed anodized / coloured layers: Bode modulus (a) and Bode phase (b).

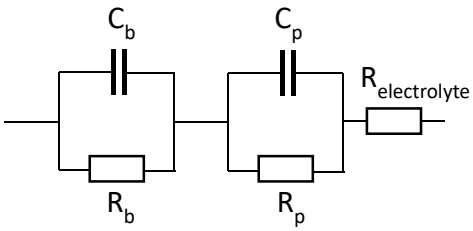

Fig. 6. Equivalent electrical circuit used to fit the EIS data of the sealed and unsealed nanoporous oxide layers.

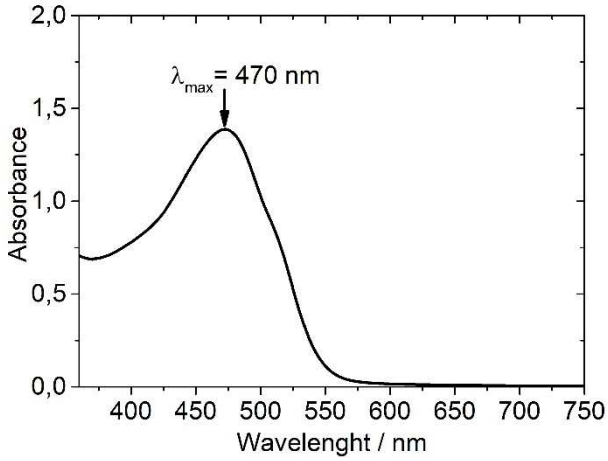

Fig. 7. Absorption UV-visible spectrum of the orange dye G.

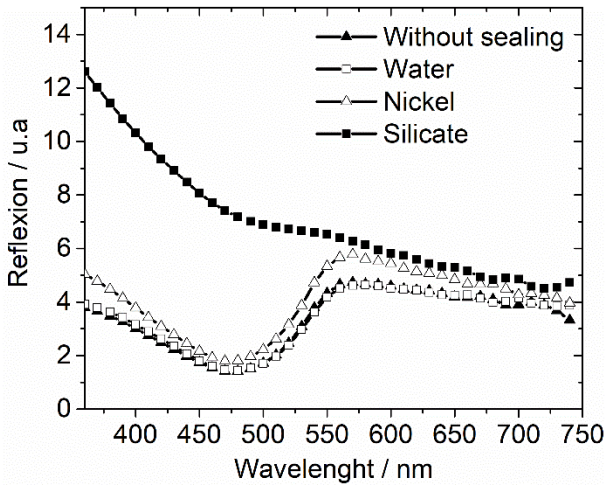

Fig. 8. UV-Visible reflection spectra recorded on unsealed and sealed layers.

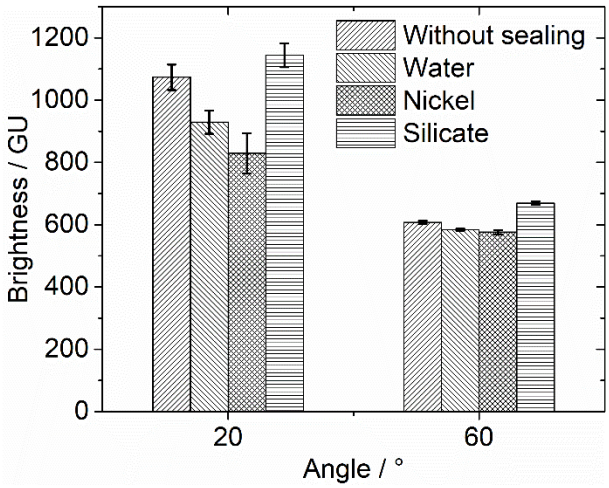

Fig. 9. Gloss measurements at two angles versus normal direction on the unsealed and sealed surfaces.